sustainability

MDPI

Article

Corrosion Evaluation of Geopolymer Concrete Made with Fly Ash and Bottom Ash

Priyanka Morla, Rishi Gupta *, Peiman Azarsa and Ashutosh Sharma

Department of Civil Engineering, University of Victoria, Victoria, BC V8W 2Y2, Canada; pmorla@uvic.ca (P.M.); azarsap@uvic.ca (P.A.); rasharma86@uvic.ca (A.S.)
* Correspondence: guptar@uvic.ca

Abstract: Environmental pollution caused by CO_2 releasing from the production of cement is a great challenge for the construction industry and has triggered exploration into more sustainable alternatives. Geopolymer Concrete (GPC) is a potential sustainable solution that does not involve the use of cement as a binder. GPC is produced by mixing the alumino-silicate source materials such as fly-ash with alkali activators such as potassium hydroxide (KOH) and potassium silicate (K_2SiO_3). Unlike Ordinary Portland Concrete (OPC), the characteristics of GPC depend on the precursor materials and therefore vary for different mixes. Consequently, corrosion behavior needs to be evaluated separately for individual mixes. This has narrowed the scope of existing published work on corrosion behavior of GPC. In this study, GPC and OPC specimens were prepared and exposed to accelerated corrosion exposure. Half-cell potential and linear polarization resistance were used to evaluate the corrosion rate in GPC and OPC. Under accelerated conditions, the corrosion rate of the GPC specimens was between 10 µm/year and 20 µm/year exhibiting a moderate to high rate of corrosion. Meanwhile, the corrosion rate of the OPC specimens was between 40 µm/year and 60 µm/year indicating a very high corrosion activity. It can be concluded that GPC has a higher resistance to chloride-induced corrosion; with a low corrosion rate and lower mass loss percentage, compared to OPC.

Keywords: sustainability; geopolymer concrete; bottom-ash; fly-ash; half-cell potential; linear polarization resistance

Citation: Morla, P.; Gupta, R.; Azarsa, P.; Sharma, A. Corrosion Evaluation of Geopolymer Concrete Made with Fly Ash and Bottom Ash. *Sustainability* **2021**, *13*, 398. https://doi.org/10.3390/su13010398

Received: 5 December 2020
Accepted: 30 December 2020
Published: 4 January 2021

1. Introduction

Green economy, biocarbon economy, and low-carbon economy are some of the terms that indicate the global efforts for decarbonization [1]. The onus is on the mitigation policies for reducing greenhouse gas emissions. The year 2017 recorded the highest inclination of the order of 32.5 Gt. carbon-dioxide emissions [2] out of which 39–28% is from the building and construction sector and 11% is from building materials and transport activities. The construction industry is a carbon-intensive sector, consuming significant amounts of energy, products, and services of different sectors, which is greatly challenging the sustainable growth [3,4]. In the entire spectrum of the construction industry, the production of cement alone produces the largest amount of carbon dioxide and is the 2nd largest source of CO_2 emissions worldwide. Henceforth, the global environmental impact of cement production has resulted in increased momentum of research for sustainable alternatives. The utilization of supplementary cementitious materials (SCM's) such as fly ash, Rice husk ash, GGBS, etc. as partial replacement of cement is being extensively explored. Their potential for enhancing the binder characteristics and reduction of environmental impact has been well recognized [5].

The exploration of a sustainable solution for a two-faced problem, i.e., reduction of CO_2 emissions and industrial waste management, has led to the development of alkali-activated concrete known as geopolymer concrete. The term 'geopolymer' was first used

in Davidovit's work on the formation of polymeric Si-O-Al bonds from the chemical reaction of alkali silicates with aluminosilicate precursors [6]. As per the Duxson model [7], the process of polymerization involves three steps: (1) the dissolution of aluminosilicate materials and the release of silicate and aluminate monomers$[Si(OH)_4]^-$ and $[Al(OH)_4]^-$; (2) Initial gels(mono cross-linked systems) are being produced by co-sharing of oxygen atoms from the reactive silicate and aluminate monomers, the process being known as condensation; (3) In the last stage the initial gels are converted into the geopolymers gels and the process is known as polycondensation. Different industrial waste materials such as fly ash, metallurgical slag, metakaolin, mining wastes, silica fume etc. could be used as source materials for geopolymerisation. Although, the reactivity depends upon their physical, chemical and morphological properties but a stable geopolymer requires the source material to possess the following characteristics: (1) highly amorphous; (2) enough reactive glassy content; (3) low-water demand; (4) ability to release aluminium easily. A more detailed model for geopolymerisation given by Provis [8], discusses the synthesis of geopolymer and zeolites by the polymerization of metakaolin and fly ash. The model explores the different silicate oligomers for their inclusion in the alkali solution. The respective oligomers polymerize into geopolymer fragments and aluminosilicate nuclei. Finally, the geopolymer gels and zeolites are formed by the polycondensation of the remaining silicate monomers. Both microstructural and the chemical properties of geopolymers with different source materials will vary greatly despite their physical properties might appear to be similar. Alkali activators, an important constituent of polymerization, are used to activate the aluminosilicates materials. The most commonly used alkali activators are sodium hydroxide, potassium hydroxide, sodium silicate, and potassium silicates [7].

After lime and Portland cement, geopolymer could be considered as the third-generation cement. Geopolymers can be modified by correctly selecting the raw materials and optimizing the design mix. The characteristics of geopolymer concrete have been reported to be better than normal concrete. Since the input materials for the geopolymer mix could be different, therefore the final products of hydration are different from those produced in the hydration of cement [9,10]. The liquid-solid ratio, SiO_2/Al_2O_3, R_2O/Al_2O_3, SiO_2/R_2O ratio majorly impacts the properties of geopolymer pastes. Numerous authors have suggested that an amorphous structure of geopolymer will result in better mechanical properties [9,11–13]. This is primarily due to the refinement of pores by the dissolution of particles and the formation of products. The reduced porosity improved the strength of the paste [11]. Along with mix-ingredients, curing conditions greatly impact the characteristics of geopolymer concrete [14–19]. Curing of geopolymer concrete can be done in three ways: (1) Heat curing; (2) Steam curing; (3) Ambient curing. The curing temperatures required for the consummation of polymerization ranges between 40–85 °C. For achieving the desired mechanical and durability characteristics, adequate curing of geopolymer concrete is required [18].

The strength of the matrix depends upon the microstructure of materials used for its production and significantly influences the permeability of the matrix. The formation of geopolymers from polymeric sodium aluminosilicate hydrate gel (N-A-S-H) differentiates it from normal concrete made from calcium silicate hydrate gel (C-S-H) [11]. Further, the low calcium content of Geopolymer concrete from that of normal concrete reduces the durability issues significantly. Hence, a differential durability behavior (design life and performance) of geopolymer concrete structures should be expected from that of normal concrete. durability Steel corrosion is one of the major issues that has impacted the long-term performance of structures made with normal concrete [20,21]. Ingress of chlorides inside concrete damages the pseudo passive layer that protects the steel from corrosion [22]. Some reports stated [23] that improving the quality of GPC can prevent the corrosion of the reinforcement bar. Tennakoon et al. [24] performed long-term tests on corrosion of steel rebar in fly-ash-based GPC and slag-based GPC. The results of their study showed that the chloride diffusion coefficient is less in fly-ash and slag GPC than that of OPC concrete. Tennakoon et al. [24] have also concluded that the embedded rebar in fly-ash and slag-based GPC has a higher resistance to corrosion than a rebar in

OPC. Reddy et al. [25] experimented on the durability of reinforced GPC in the marine environment. Reddy et al. [26] evaluated the corrosion-based durability of low calcium fly-ash-based GPC using beams that are centrally reinforced, made with 8M and 14M concentrations sodium-based solutions. The experimental results proved that GPC has better corrosion resistance performance compared to OPC. Regarding the corrosion of reinforcement in GPC, the literature is relatively limited; there are a few work reported on corrosion resistance evaluation of steel rebar in fly-ash based GPC [27,28].

From a safety perspective, it is essential to perform routine assessments of concrete to identify the damages in the areas with critical levels of corrosion [22]. There are many destructive methods for corrosion assessment of GPC structure, which requires material samples to be taken from the structure. In this regard, Non-Destructive Testing (NDT) methods must be deployed for testing without destroying the structure [29,30]. The only standardized test methods for corrosion monitoring is the half-cell potential technique given by [31]. Hence, measurement of steel corrosion in GPC using two NDT methods, half-cell potential and linear polarization resistance, can be an effective indicator of steel reinforcement corrosion rate. In one of the studies, researchers have used half-cell potential and linear polarization resistance method to experimentally study the corrosion rate of steel rebar in GPC produced from three types of fly-ashes over 540 days of exposure to 3% sodium chloride (NaCl) solution [32]. The corrosion rate values for these GPCs ranged from 0.55 to 1.65 $\mu A/cm^2$ where these findings were almost equal to conventional concrete (0.65–1.20 $\mu A/cm^2$). In another study, it was stated that half-cell potential values for the passivated reinforcement in GPC (ranging between −100 to −200 mV) is moderately similar to the OPC mortar results [33].

Due to different precursor materials such as fly ash, Metakaolin, granulated blast furnace slag, etc., the hydration of cement and the polymerization process in geopolymer vary significantly. As a result, the characteristics of geopolymer concrete such as the microstructure, mechanical behavior, and durability vary considerably. Hence, it is important to evaluate the overall characteristics of a precursor based geopolymer concrete before it can be used for construction. Several studies have reported the use of fly ash as a precursor and bottom ash as a replacement of fine aggregates for developing geopolymer concrete. However, corrosion evaluation of geopolymer concrete made with both fly ash and bottom ash precursor material has been rarely reported. The focus of this paper is to develop a sustainable fly-ash based geopolymer concrete with a 50% replacement of bottom ash. Further, the durability behavior of the matrix in terms of resistance to chloride-induced corrosion in comparison with ordinary concrete is also investigated. Two non-destructive techniques i.e., Half-cell potential and Linear Polarization resistance, have been employed to study the corrosion behavior.

2. Experimental Program

2.1. Precursor Material

Three classes of fly-ash (class N, F, C) are desired for use in GPC mix design. In the production of K-based GPC, class F fly-ash as a pozzolanic material was obtained from Lafarge Cement, Vancouver, BC, Canada. Bottom-ash used in this study was also supplied by Lafarge Cement, Vancouver, BC, Canada. This bottom-ash was obtained from the pulverized coal combustion. The major components in bottom-ash are Silicon Oxide (SiO_2), Aluminum Oxide (Al_2O_3), and Iron Oxide (Fe_2O_3). Magnesium Oxide (MgO), Calcium Oxide (CaO), Sodium Oxide (Na_2O), and Potassium Oxide (K_2O) are also detected and are present in small quantities. The chemical composition of both fly-ash and bottom-ash are shown in Table 1.

2.2. Alkali Activator

A combination of K_2SiO_3 and KOH was used as the alkaline activator. KOH was obtained from Sigma-Aldrich, Ontario (Canada) with >85% purity in ACS grade. This was supplied in flakes form. The KOH solution was prepared by dissolving the flakes in water.

The mass of KOH solids in a solution varies depending on the concentration of the solution expressed in terms of a molar, M. The concentration of KOH used was 12 Molar. The KOH solution was prepared 24 h in advance of use by dissolving measured KOH pellets in the required amount of tap water.

Table 1. Chemical composition of by-products.

Compound	Fly-Ash (%)	Bottom-Ash (%)
SiO_2	47.1	60.11
Al_2O_3	17.4	14.35
Fe_2O_3	5.7	5.92
CaO	14	10.40
MgO	5.4	4.49
SO_3	0.8	0.10
Na_2O	N/A	2.232
K_2O	N/A	1.766
TiO_2	N/A	0.892
P_2O_5	N/A	0.200
Mn_2O_3	N/A	0.093

K_2SiO_3 powder (AgSil16H) was obtained from PQ Corporation, Philadelphia (USA) was used in this project. Based on the Material Safety Data Sheet (MSDS) provided by the company, the chemical composition of the K_2SiO_3 powder was K_2O = 32.4%, SiO_2 = 52.8%, and water weight percentage of 14.8%.

2.3. Ordinary Portland Cement

Type 1 Portland cement was used for the manufacture of the control mix concrete. The control concrete mix was designed to have a target strength of 35 MPa similar to that of GPC.

2.4. Aggregates

Fine aggregates and coarse aggregates used were obtained from a quarry in British Columbia with a relative dry density of 2.671 and 2.713 respectively, and a water absorption ratio of 0.79% and 0.69% respectively. The local aggregates comprising 12.5 mm were used as coarse aggregates in GPC and the aggregates comprising 12.5 mm and 6.5 mm were used in OPC; the fine aggregates used in both OPC and GPC were medium-coarse sand which was suitable for multipurpose use including concrete mixtures.

3. Method of Casting and Curing

3.1. Specimen Dimensions

In this study, the mix proportion and curing method of GPC build on previous work done in the Facility for Innovative Materials and Infrastructure Monitoring (FIMIM) by the authors [34–36]. Three specimens of RC beams of dimensions 152 mm × 152 mm × 533 mm were cast using GPC (named as GPC-1, GPC-2, GPC-3) and the other three were made with OPC (named as OPC-1, OPC-2, and OPC-3). A reinforcing steel rebar of diameter 12.5 mm was also embedded inside the concrete beam.

3.2. Specimen Preparation

The alkali solution was prepared 24 h before casting day. Then, the solid constituents of GPC, i.e., the aggregates, fly-ash, and bottom-ash were first mixed in the dry condition in a rotary drum mixer for about 1 min. Next, the alkali solution was added to the solids and mixed for about 3 min, followed by a 3 minutes' rest period, then followed by 2 min of final mixing. The mixture was placed into molds and vibrated using a table vibrator for 30 s to discharge air bubbles to the surface. Then, the molds were covered with a plastic sheet in a lab environment (approximate relative humidity range of 45% to 70% and approximate

temperature range of 5 °C to 15 °C); demolded after 24 h. GPC beams were placed into a tray filled with water and were then kept in an oven at a temperature of 80 °C for 24 h. After that, the specimens were cured at ambient temperature for 28 days.

The mix proportions of GPC beams (obtained from previous work performed by authors) and OPC beams are shown in Tables 2 and 3 respectively.

Table 2. Mix design of GPC.

Material	Content (kg/m^3)
Fly-ash	194
Bottom-ash	194
Coarse aggregates	1170
Sand	630
KOH (12M)	85.16
K_2SiO_3	125.74

Table 3. Mix proportion of OPC.

Material	Content (kg/m^3)
Cement	400
Sand	660
12.5 mm aggregate	701
6.5 mm aggregate	467
Water	160

To prepare the OPC beams, the dry ingredients such as cement, sand, and coarse aggregates were mixed for about 2 min and the water was added slowly until the concrete was uniform and workable. After compaction on a vibrator table, each beam was labeled and then covered with a plastic sheet to prevent evaporation and kept overnight in the laboratory at ambient temperature. The OPC samples were de-molded and stored in a water tank at 23 ± 2 °C for 28 days. Further, a steel rebar of nominal diameter 12.5 mm and length 650 mm was embedded in concrete in such a way that 100 mm of the total length remained exposed. Commercially available hot rolled steel reinforcing bars with a yield strength of 400 MPa were used. The rebar was protruded so that a connection could be made for impressed current corrosion. The embedded rebar was corrosion-free during casting. After rolling, the rebar was kept in oil. Thereafter, acetone was used to clean the rebar of oil before embedding it into the concrete. The rebar was weighed to the accuracy of 1 g. To prevent the crevice corrosion at the steel-concrete interface and to serve as a bond breaker, the rebar was wrapped with Teflon tape. The protruded 100 mm length of the rebar was epoxy coated to protect from the corrosive environment.

4. Methodology

After 28 days, when GPC and OPC samples cured in ambient temperature and water tank respectively, beams were placed in a chloride solution for 28 days. This helps to keep the initial D.C. power to a manageably low value. Figure 1 is a schematic of the accelerated corrosion test setup in 5% NaCl solution used in this work. As can be seen in Figure 1, the corrosion tank was filled with chloride solution that would allow each beam to be partially immersed. After that, the extended side of the rebar acting as an anode was connected to a 30 V power supply. A stainless-steel rod was used to act as a cathode. The D.C. power supply was turned on and set to 30 V electrical potential. This voltage was chosen based on work conducted by [26] to make the steel rebar as anodes, accelerate the corrosion process, and decrease the test period time.

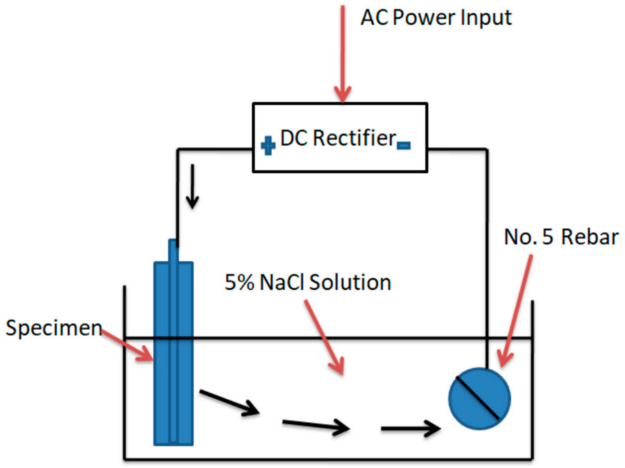

Figure 1. Schematic test set-up of accelerated corrosion exposure to OPC and GPC specimens.

Once the testing procedure started, current readings were taken every 24 h. A rise in the current indicated the beginning of the corrosion process, and eventually the start of the formation of cracks in the beams. Once the beams reached a high current value, there were visible signs of corrosion and cracking of beams and the beams were considered to be failed. The time taken to initiate the corrosion in the rebar in GPC was higher than that of OPC concrete. The beams were removed from the chloride water and left to air dry for 24 h. After that, the beams were tested for the rate of corrosion using Linear Potential Resistance. The final step involved splitting the OPC and GPC beams to recover the rebar and to determine the effects of corrosion on the rebar by measuring the mass loss of the steel rebar in each beam.

4.1. Half-Cell Potential

Half Cell Potential (HCP) is an effective method that has been used by many researchers across the world [37–39]. Further [31] provides the guidelines for predicting corrosion activity (Table 4). It is a method of assessing the invisible corrosion of reinforced concrete without destructing the samples. HCP provides information about the probability of corrosion. Table 4 gives the guide for evaluation of corrosion activity versus a standard copper/copper sulfate half-cell.

Table 4. Predicting corrosion using Cu/CuSO4 half-cell [31]

Corrosion Risk	Half-Cell Potential (Versus $Cu/CuSO_4$)
Severe Corrosion	Less than −500 mV
High Corrosion Risk (90% probability)	Between −500 mV & −350 mV
Medium corrosion risk (50% probability)	Between −350 mV & −200 mV
Low Corrosion Risk (10% probability)	Higher than −200 mV

Figure 2 indicates a schematic of the HCP measurement setup. In accordance with [31], a digital voltmeter is used to read the potential difference values between the external reference electrode and the reinforced steel rebar. In this study, copper/copper sulphate was used as a reference electrode. If the surface of the concrete is too dry, pre-wetting is required. A pre-wetted sponge is used to ensure proper surface contact between the concrete surface and the tip of the half-cell electrode.

For a consistent reading, a centerline with a pre-defined equal spacing of three measuring points at a 175 mm distance was marked on the surface of the concrete. The potential values for these three points were recorded from the voltmeter for both OPC and GPC beams.

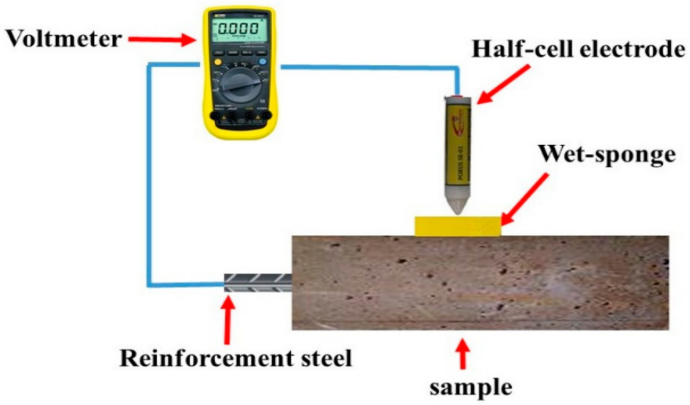

Figure 2. Schematic test set-up of the HCP measurements of OPC and GPC specimens.

4.2. Linear Polarization Resistance

The Linear Polarization Resistance (LPR) method is a non-destructive testing method used to measure the corrosion rate. The data graph obtained from the instrument can be used to calculate the corrosion rate. Polarization resistance measurements are an accurate and rapid technique to measure the rate of corrosion. Typical values relating corrosion measurements to predicted corrosion penetration are given in Table 5.

Table 5. Values of corrosion measurements [40].

Rate of Corrosion	Polarisation Resistance R_P (Ω cm^2)	Corrosion Current Density I_{CORR} (μA/cm^2)	Corrosion Penetration p (μm/Year)
Very high	2.5–0.25	10–100	100–1000
High	25–2.5	1–10	10–100
Low/moderate	250–25	0.1–1	1–10
Passive	>250	<0.1	<1

After the specimens were removed from the chloride water and left to air dry for 24 h, the LPR test was performed. The specimens were supported on a wooden surface. To conduct the LPR test, Gamry Instruments Reference 600+ potentiostat was used. The cell cable was connected to a reference electrode, counter electrode, rebar, and ground. If the surface of the concrete was too dry, samples were pre-wetted. A pre-wetted sponge was used to ensure proper surface contact between the concrete surface and the tip of the reference electrode. The equipment was connected to a computer to read the data graph. A complete setup of the Gamry potentiostat is shown in Figure 3. The Gamry Echem Analyst software was used to run the experiment. This is a single program that runs data-analysis for all types of experiments such as DC corrosions, EIS, and physical electrochemistry. Before running the software, the experimental setup values are entered manually (Table 6).

Same as the HCP technique, a centerline with a pre-defined equal spacing of three measuring points at 175 mm distance was marked on the surface of the concrete to obtain a set of reliable test values. The LPR data graphs for these three points were recorded in the computer for both OPC and GPC beams. The values shown in Table 6 were used in the LPR measurement:

B value is often taken as 25 mV for active corrosion state and 50 mV for passive conditions [41]. E_w is the equivalent weight of the corroding metal.

The corrosion rate can be computed by using the corrosion current (I_{CORR}) generated by the flow of electrons from anode to cathode. By applying the modified version of Faraday's law, the following equation can be generated

$$I_{CORR} = \left(10^6 B\right) / R_p \ \left(\mu \mathrm{A/cm^2}\right) \quad (1)$$

where R_p is the polarization resistance of a corroding electrode and is defined as the slope of potential versus current density plot. The dimension of R_p is ohm-cm^2.

B is the Stern-Geary coefficient and the Stern-Geary coefficient is given by

$$B = b_a b_c / [2.303(b_a + b_c)] \quad (2)$$

where b_a and b_c are the anodic and cathodic Tafel slopes.

The corrosion rate in μm per year is given by

$$CR = 3.27 \cdot I_{CORR} \cdot (E_w / \rho) \quad (3)$$

where: I_{CORR} = Corrosion current density in μA/cm^2, E_w = Equivalent weight of the corroding metal, ρ = density of the corroding metal in g/cm^3.

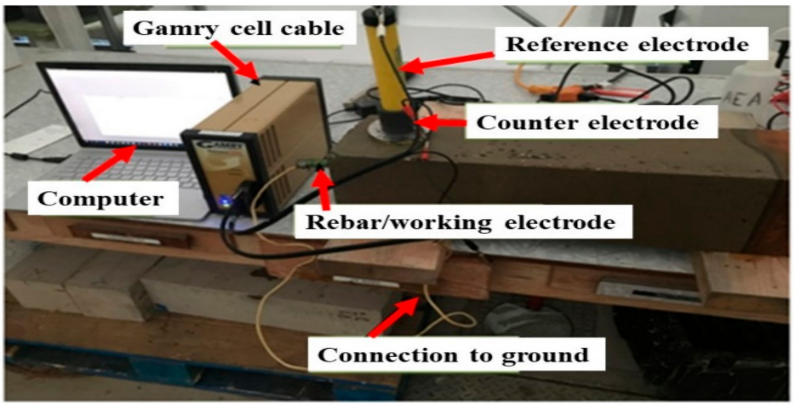

Figure 3. Gamry potentiostat set-up for linear polarisation measurements.

Table 6. Values input in the software.

E_w	Density (ρ)	B
27.92	7.85 g/cm^2	25 mV

5. Results and Discussion

5.1. Compressive Strength

As aforementioned, this section builds on the previous work on the effect of the curing regime on compressive strength of GPC performed by authors [34–36]. To maintain brevity, this previous work is briefly described here. Authors used steam curing and dry curing methods to accelerate curing of cylindrical GPC specimens (of size (100 mm × 200 mm) at five different temperatures including ambient, 30 °C, 45 °C, 60 °C, 80 °C. According to the previous results, the highest compressive strength (35 MPa at an age of 28 days) was obtained at a temperature of 80 °C of steam curing for the abovementioned mix proportion, possibly due to the full and uniform internal curing of steam cured specimens. Hence, in the present study, the cylindrical GPC and OPC specimens were steam cured and were tested at 7 and 28 days. A minimum of three GPC and three OPC specimens were used in this test. The average compressive strength of GPC specimens at 7 and 28 days was 26.65 MPa and 31.70 MPa respectively.

For the OPC, the average strength of the three samples was 26.93 MPa and 33.67 MPa at 7 and 28 days respectively. As the age was increased from 7 to 28 days, the compressive strength of GPC and OPC samples increased by 18.95% and 25.03% times respectively. It can be concluded from the results that GPC steam cured at 80 °C for 24 h developed almost an equal strength as the OPC samples cured for 28 days. More importantly, these two mixes

were considered comparable for the rest of the research conducted in this work. The mix proportion selected after compression testing of GPC cylindrical samples was used for the production of GPC beams. Also, it should be noted that failed OPC specimens exhibited cracked paste and aggregate interface whereas the GPC exhibited plain surfaces of failure. This further indicates that the bond formed between the binder and the aggregates was stronger than OPC specimens. Figure 4 shows the compressive strength of GPC and OPC at age of 7 and 28 days.

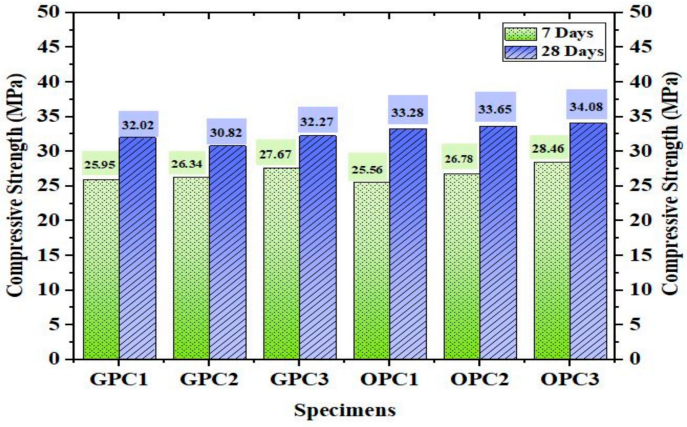

Figure 4. 28th-day compressive strength of GPC and OPC.

5.2. NDT Evaluation

5.2.1. Visual Inspection

The accelerated corrosion test was terminated at 300 h and the beams were removed from the chloride solution tank. Figure 5a,b shows the corroded OPC and GPC specimens after nearly 200 h of the test. The OPC beams started to show signs of rusting after 60 h of accelerated corrosion exposure. On the other hand, the GPC beams showed no signs of rust for the same period. The brown rust stain seen on OPC beams was the first visual evidence of corrosion in the embedded steel. At this stage, it was also observed that corrosion products were floating on the surface of the chloride solution. After nearly 200 h, a crack was observed in the OPC beams. From this point onwards, the crack propagated longitudinally parallel to the length of the bar. After 300 h of corrosion exposure, along with a horizontal crack, a vertical crack was also observed which became wider under flexure. On the other hand, there were no cracks observed in the GPC beams indicating better corrosion resistance when compared to OPC beams. GPC specimens exhibited superior durability characteristics than OPC specimens.

(**a**) OPC Specimen (**b**) GPC specimen

Figure 5. (**a**) OPC beam after 200 h of accelerated corrosion exposure, (**b**) GPC beam after 200 h accelerated corrosion exposure.

5.2.2. HCP Analysis

Before performing the accelerated corrosion test, the initial HCP readings on day 1 were taken from the voltmeter for both OPC and GPC beams. There were three measurement points on each specimen, and the potential values for these three points were recorded and then averaged. These readings were taken on alternate days until the test reached 300 h. Figure 6 represents the average HCP values of GPC and OPC specimens. The corrosion process is divided into three stages of propagation i.e., from first 0–3 days as stage 1, from 4 to 8 days as stage 2, and 8 to 13 days as stage 3. From Figure 6, it is evident that GPC samples exhibited passivity in stage 1 whereas OPC samples exhibited 50% corrosion likelihood with its potential values ranging from −100 mV to −230 mV. Figure 6 also includes the [31] standard for evaluation of corrosion activity. Stage 2 indicates that while GPC samples indicate the minimal likelihood of corrosion activity, the OPC samples still indicate a 50% likelihood of corrosion with its potential values ranging from −250 to −300 mV. Further in Stage 3, GPC samples exhibit a 90% probability of corrosion on day 13 while OPC samples exhibit the same on the 7th day. This clearly distinguishes the fact that GPC offers better resistance to chloride induced-damage than OPC. It can be seen that the drop in potential from day 0 to 3 is very less as it falls after the 4th day. This is attributed to the fact that a layer of rust gets developed around the rebar that protects it from corrosion progression for a while. As corrosion products build-up, iron ions easily diffuse through the layer of rust and results in a sharp drop of corrosion potential and quick progression of corrosion. Although, the HCP measurements cannot be directly related to corrosion rate it surely signifies the trend of corrosion progression. Furthermore, it indicates that the rate at which chlorides come in contact with a steel bar in case OPC is far lesser in GPC, indicating extra passivation provided by GPC [26,42,43].

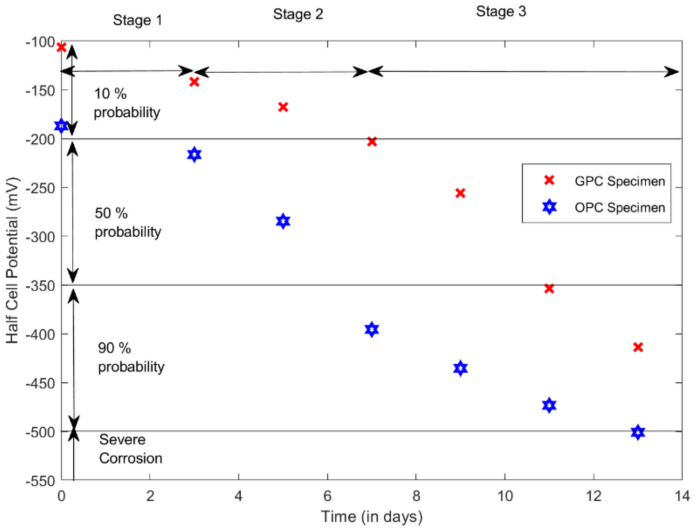

Figure 6. Variation of Half−Cell potential measurements with time for OPC and GPC specimens.

5.2.3. LPR Analysis

The LPR technique is used for accurately measuring the corrosion rates of the specimens and the results are tabulated in Table 7. The corrosion rate is calculated by using the equations discussed in Section 2. The experiments are conducted for GPC specimens and OPC specimens using Gamry potentiostat. The average LPR values of three GPC and three OPC specimens are shown in Figure 7a,b. It can be seen that the recorded half-cell potential of GPC showed higher average values ranging from −380 mV to −415 mV than OPC (−427 mV to −470 mV). The average LPR of GPC decreased by −8.32% when Im (A) changed from 20 µA to −20 µA whereas the average LPR of OPC decreased −9.9% at the same Im (A) range.

Table 7. LPR resistance test results.

S.NO.	Specimen	Corrosion Current I_{CORR} (μA/cm^2)	Corrosion Rate (μm/Year)	Corrosion Condition
1.	GPC 1	0.9113	10.598	Moderate
2.	GPC 2	1.2303	14.308	High
3.	GPC 3	1.7429	20.270	High
4.	OPC 1	4.9214	57.233	Very high
5.	OPC 2	4.1010	47.696	Very high
6.	OPC 3	5.0471	58.698	Very high

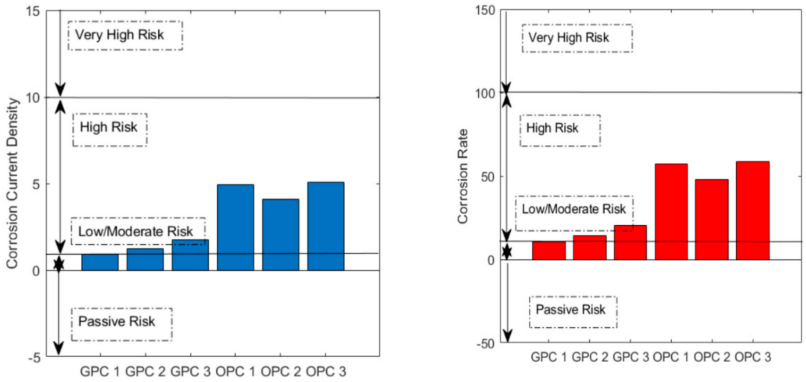

(**a**) Corrosion current density (**b**) Corrosion rate

Figure 7. (**a**,**b**) Mean linear polarisation values for OPC and GPC samples exposed to corrosion.

Based on the LPR measurements, Figure 7a,b has been categorized into passive, low moderate, high, and very high risks, as per [44]. From Figure 8, it is evident that the corrosion rate of the GPC specimens is between 10 μm/year and 20 μm/year. This indicates that these specimens have a moderate to high rate of corrosion. No cracks were observed on the surface of the GPC specimen, but micro-cracks may have occurred in the surrounding areas of the bar due to the corrosion products that was built up inside, which might have allowed some chloride ions to penetrate the vicinity of the bar. As compared to this, the corrosion rate of the OPC specimens is between 40 μm/year and 60 μm/year, indicating a very high risk of corrosion.

Figure 8. Corroded GPC and OPC specimens after 200 h of accelerated corrosion exposure.

6. Destructive Tests

6.1. Mass Loss Measurements

The corrosion assessment of steel bars used in the reinforced concrete can also be done by mass loss measurements [26,45]. The initial mass of each rebar is recorded before the casting procedure. After the corrosion exposure was completed, the beams were completely broken to extract the entire rebar (Figure 8).

The rebars were cleaned with deionized water and a metal brush was used to remove the corrosion products from the rebars. The steel rebars visually showed critical corrosion damage for the OPC beams, while the rebars from the GPC beams showed less damage compared to OPC beams. The rebars extracted from the beams were weighed and recorded as the final mass. Then the percentage of mass loss was calculated for rebars both in OPC and GPC beams as per [46].

Table 8 shows the percentage mass loss of three GPC and three OPC specimens. The percentage mass loss for the GPC beams was 3.13%, 4.13%, and 5.16% respectively, whereas, for the OPC beams it is significantly higher at 21.80%, 16.73%, and 19.52% respectively. The OPC beams showed significant mass loss due to the early crack formation which allows the chloride ions to penetrate quickly into the concrete and increase the rate of corrosion.

Table 8. Mass loss in rebar in GPC and PCC.

Specimen	Initial Mass (gms)	Final Mass (gms)	Mass Loss (%)
GPC 1	944.5	914.9	3.13
GPC 2	945.5	906.4	4.13
GPC 3	941.9	894.5	5.16
OPC 1	941.9	756.8	21.80
OPC 2	944.3	786.3	16.73
OPC 3	943.7	759.4	19.52

This finding is in good agreement with those obtained in previous studies [24,45,47]. Several factors such as low permeability, high alkalinity, improved microstructure matrix, etc. significantly enhance the corrosion resistance of GPC to aggressive exposure to chlorides.

6.2. Residual Flexural Strength

Corrosion of reinforcement affects the load-carrying capacity of any RC structure as it reduces the cross-section of rebar that ultimately results in cracking and spalling of concrete. Therefore, it is imperative to study the residual strength of structures after corrosion-induced damage has been taken place. This provides an in-depth- understanding and insight into the kind of rehabilitation measures that could be utilized for restoring the integrity of the structure. After HCP and LPR testing, the specimens were tested in flexure under 3-point loading using an MTI-K testing machine as per [48]. The residual flexural strength values are given in Table 9**.** From Table 9, it can be observed that the GPC beam specimens exhibit improved flexural behavior than those of OPC specimens. Hence, it can be ascertained that under similar corroding exposure, the load-carrying capacity of GPC remains intact for a longer period.

Table 9. Residual Flexural Strength test values.

Specimen	Residual Flexural Strength (in MPa)
GPC-1	5.1
GPC-2	4.8
GPC-3	4.4
OPC-1	3.9
OPC-2	3.7
OPC-3	3.65

7. Discussion

Table 10 gives the average values of 7 & 28-day compressive strength, mass-loss, corrosion current and corrosion rate, and average flexural residual strength for all tested GPC as well as OPC samples. There is no significant variation of compressive strength values but there is a significant influence of corrosion exposure on OPC and fly ash based GPC with additions of bottom ash. Normally, the compressive strength values of fly ash based GPC is 5–7% higher than those of OPC [49], the similar values could be attributed to the addition of bottom ash and its replacement with fly ash itself. The larger particle size of bottom ash will have some effect on the densification of the matrix and consequently, the loss of compressive strength is observed. The various parameters such as pore size, connectivity of pores, shrinkage and movement cracks, chemical characteristics i.e., the chloride binding capacity, alkalinity [50,51] largely control the dynamics of corrosion of steel in concrete. The durability of a mix majorly depends upon its mineralogical constituents and microstructure [52]; the difference between the reaction products of OPC and GPC could significantly alter their characteristics. Despite the addition of bottom ash, the GPC mix has exhibited significant corrosion resistance than the OPC samples. GPC samples exhibited 78% less mass-loss, 72% lower corrosion rate and 73% lesser corrosion current density. Further, the residual flexural strength is 21% higher than those of OPC samples. The corrosion-resistant behavior of GPC is probably because of the refinement of pore structures as an outcome of polycondensation reaction and therefore, the filler effect. This further reduces the porosity of the GPC mix as the presence of KOH aids in leaching of Si and Al from fly ash improving the polycondensation and the matrix. The densification of the GPC matrix with reduced permeability and improved strength will restrict the ingress of chloride ions into the steel-concrete ecosystem. This reduces the chloride-diffusion rate in GPC mix as compared to OPC mix which is directly evident from the reduced corrosion current (I_{CORR}) and corrosion rate as well. The reduced mass-loss and less influence of corrosion exposure on GPC could also be attributed to the reduced availability of free chlorides and therefore, increased chloride binding capacity. The slope obtained from the regression of HCP measured values suggests that the rate of drop in potential was much higher for OPC samples than GPC samples. In a study [42], researchers have also suggested lesser HCP for fly ash based GPC than ordinary concrete. Previous studies have shown that GPC undergoes lesser deterioration due to corrosion exposure and the time of failure is prolonged for more than 3.5 times than the OPC [47]. In addition to the denser matrix due to the presence of fly ash and bottom ash than that of OPC, the presence of alkaline activators significantly improves the electrical resistance due to the increased availability of ions [32,47,52]. From Table 10, a clear correlation between all the evaluated corrosion parameters suggests GPC offers enhanced resistance to chloride-induced corrosion.

Table 10. Average Test results.

Specimen Details	Avg.7day Compressive Strength	Avg.28day Compressive Strength	Average Mass-Loss	Average Corrosion Rate	Average Corrosion Current	Average Residual Flexural Strength	Slope of HCP
OPC	26.93	33.67	19.52	54.54	4.689	3.81	28.6
GPC	26.65	34.22	4.14	15.06	1.294	4.86	20.4
%age Diff	−1.03	1.6	−78	−72	−73	21	

8. Conclusions

The primary aim of this study was to experimentally study the corrosion resistance of sustainable bottom-ash and fly-ash based reinforced GPC, compared to OPC. The study has shown a promise to the use of a combination of fly ash and bottom ash as precursor materials for developing GPC by analyzing the test results, the following conclusions can be drawn.

- The geopolymerised fly ash and bottom ash based concrete exhibited more homogeneity and superior aggregate-binder bond than OPC. Additionally, the compressive strength of both GPC and OPC were comparable.
- The drop in the HCP readings indicated a much-delayed depassivation of GPC samples than those of OPC samples. It also indicated a lower permeability, high alkalinity of GPC specimens in aggressive corrosive environments.
- GPC demonstrated lower values for corrosion rate compared to OPC because GPC has a moderate to high rate (between 10 μm/year and 20 μm/year). Whereas OPC showed a higher rate of corrosion (40 μm/year and 60 μm/year). The longer service life of GPC in aggressive environments can be inferred from OPC.
- Visual investigations suggested that cracking in OPC started after 60 h of accelerated corrosion exposure. Both horizontal and vertical cracks were observed in the OPC whereas no crack was observed in GPC until the end of corrosion exposure. From the drop in potential values, it can be ascertained that there was a development of micro-cracks in geopolymer concrete also.
- OPC showed higher average mass loss (19.15%) compared to GPC (4.14%). This is primarily due to the lower chloride penetrability due to better microstructure provided by finer fly ash particles and also the higher electrical resistance provided by available ions in GPC
- This study has shown a few properties of GPC to enable its use as a sustainable building material. GPC possesses a higher resistance to the corrosive activity of salt solutions compared to OPC.

Author Contributions: Conceptualization, R.G. and P.M.; methodology, P.A.; software, A.S.; validation, P.A., and P.M., formal analysis, A.S.; investigation, P.M. and P.A.; resources, R.G.; data curation, A.S.; writing—original draft preparation, P.A.; writing—review and editing, R.G. and A.S.; visualization, P.A.; supervision, R.G.; project administration, R.G.; funding acquisition, R.G. All authors have read and agreed to the published version of the manuscript.

Funding: Funding in part by India-Canada IMPACTS Centre of Excellence and Natural Sciences and Engineering Research Council of Canada.

Institutional Review Board Statement: Not Applicable.

Informed Consent Statement: Not applicable.

Data Availability Statement: The data presented in this study are available on request from the corresponding author. The data are not publicly available due to the continuation of research and other manuscripts that are in process.

Acknowledgments: The authors wish to express their appreciation to Matt Dalkie, technical service engineer at Lafarge Cement Company, and staff in the mechanical and civil engineering department at the University of Victoria for their participation in the discussion and support during the experiment phase.

Conflicts of Interest: The authors declare no conflict of interest.

References

1. Holmgren, S.; Pever, M.; Fischer, K. Constructing Low-Carbon Futures? Competing Storylines in the Estonian Energy Sector's Translation of EU Energy Goals. *Energy Policy* **2019**, *135*, 111063. [CrossRef]
2. Huang, L.; Krigsvoll, G.; Johansen, F.; Liu, Y.; Zhang, X. Carbon Emission of Global Construction Sector. *Renew. Sustain. Energy Rev.* **2018**, *81*, 1906–1916. [CrossRef]
3. Hung, C.C.W.; Hsu, S.-C.; Cheng, K.-L. Quantifying City-Scale Carbon Emissions of the Construction Sector Based on Multi-Regional Input-Output Analysis. *Resour. Conserv. Recycl.* **2019**, *149*, 75–85. [CrossRef]
4. Zhang, X.; Wang, F. Hybrid Input-Output Analysis for Life-Cycle Energy Consumption and Carbon Emissions of China's Building Sector. *Build. Environ.* **2016**, *104*, 188–197. [CrossRef]
5. Aleem, M.A.; Arumairaj, P.D. Geopolymer Concrete–a Review. *Int. J. Eng. Sci. Emerg. Technol.* **2012**, *1*, 118–122. [CrossRef]
6. Davidovits, J. Geopolymers. *J. Therm. Anal.* **1991**, *37*, 1633–1656. [CrossRef]
7. Duxson, P.; Fernández-Jiménez, A.; Provis, J.L.; Lukey, G.C.; Palomo, A.; van Deventer, J.S.J. Geopolymer Technology: The Current State of the Art. *J. Mater. Sci.* **2007**, *42*, 2917–2933. [CrossRef]

8. Provis, J.L. Modelling the Formation of Geopolymers. Ph.D. Thesis, University of Melbourne, Melbourne, Australia, 2006.
9. Van Deventer, J.S.J.; Provis, J.L.; Duxson, P.; Lukey, G.C. Reaction Mechanisms in the Geopolymeric Conversion of Inorganic Waste to Useful Products. *J. Hazard. Mater.* **2007**, *139*, 506–513. [CrossRef]
10. Provis, J.L.; Duxson, P.; Van Deventer, J.S.J.; Lukey, G.C. The Role of Mathematical Modelling and Gel Chemistry in Advancing Geopolymer Technology. *Chem. Eng. Res. Des.* **2005**, *83*, 853–860. [CrossRef]
11. De Vargas, A.S.; Dal Molin, D.C.; Vilela, A.C.; Da Silva, F.J.; Pavao, B.; Veit, H. The Effects of Na2O/SiO2 Molar Ratio, Curing Temperature and Age on Compressive Strength, Morphology and Microstructure of Alkali-Activated Fly Ash-Based Geopolymers. *Cem. Concr. Compos.* **2011**, *33*, 653–660. [CrossRef]
12. Zhang, B.; MacKenzie, K.J.; Brown, I.W. Crystalline Phase Formation in Metakaolinite Geopolymers Activated with NaOH and Sodium Silicate. *J. Mater. Sci.* **2009**, *44*, 4668–4676. [CrossRef]
13. Van Jaarsveld, J.; Van Deventer, J.S.J. Effect of the Alkali Metal Activator on the Properties of Fly Ash-Based Geopolymers. *Ind. Eng. Chem. Res.* **1999**, *38*, 3932–3941. [CrossRef]
14. Heah, C.Y.; Kamarudin, H.; Bakri, A.M.M.A.; Binhussain, M.; Luqman, M.; Nizar, I.K.; Ruzaidi, C.M.; Liew, Y.M. Effect of Curing Profile on Kaolin-Based Geopolymers. *Phys. Procedia* **2011**, *22*, 305–311. [CrossRef]
15. Rovnaník, P. Effect of Curing Temperature on the Development of Hard Structure of Metakaolin-Based Geopolymer. *Constr. Build. Mater.* **2010**, *24*, 1176–1183. [CrossRef]
16. Kani, E.N.; Allahverdi, A. Effects of Curing Time and Temperature on Strength Development of Inorganic Polymeric Binder Based on Natural Pozzolan. *J. Mater. Sci.* **2009**, *44*, 3088–3097. [CrossRef]
17. Perera, D.S.; Uchida, O.; Vance, E.R.; Finnie, K.S. Influence of Curing Schedule on the Integrity of Geopolymers. *J. Mater. Sci.* **2007**, *42*, 3099–3106. [CrossRef]
18. Van Jaarsveld, J.G.S.; van Deventer, J.S.J.; Lukey, G.C. The Effect of Composition and Temperature on the Properties of Fly Ash- and Kaolinite-Based Geopolymers. *Chem. Eng. J.* **2002**, *89*, 63–73. [CrossRef]
19. Palomo, A.; Grutzeck, M.W.; Blanco, M.T. Alkali-Activated Fly Ashes: A Cement for the Future. *Cem. Concr. Res.* **1999**, *29*, 1323–1329. [CrossRef]
20. Sharma, A.; Sharma, S.; Sharma, S.; Mukherjee, A. Ultrasonic Guided Waves for Monitoring Corrosion of FRP Wrapped Concrete Structures. *Constr. Build. Mater.* **2015**, *96*, 690–702. [CrossRef]
21. Sharma, A.; Sharma, S.; Sharma, S.; Mukherjee, A. Monitoring Invisible Corrosion in Concrete Using a Combination of Wave Propagation Techniques. *Cem. Concr. Compos.* **2018**, *90*, 89–99. [CrossRef]
22. Hong, S.; Lai, W.-L.; Helmerich, R. Experimental Monitoring of Chloride-Induced Reinforcement Corrosion and Chloride Contamination in Concrete with Ground-Penetrating Radar. *Struct. Infrastruct. Eng.* **2015**, *11*, 15–26. [CrossRef]
23. Asmara, Y.P.; Siregar, J.P.; Tezara, C.; Nurlisa, W.; Jamiluddin, J. Long Term Corrosion Experiment of Steel Rebar in Fly Ash-Based Geopolymer Concrete in NaCl Solution. *Int. J. Corros.* **2016**, *2016*. [CrossRef]
24. Tennakoon, C.; Shayan, A.; Sanjayan, J.G.; Xu, A. Chloride Ingress and Steel Corrosion in Geopolymer Concrete Based on Long Term Tests. *Mater. Des.* **2017**, *116*, 287–299. [CrossRef]
25. Reddy, M.S.; Dinakar, P.; Rao, B.H. Mix Design Development of Fly Ash and Ground Granulated Blast Furnace Slag Based Geopolymer Concrete. *J. Build. Eng.* **2018**, *20*, 712–722. [CrossRef]
26. Reddy, D.V.; Edouard, J.-B.; Sobhan, K. Durability of Fly Ash–Based Geopolymer Structural Concrete in the Marine Environment. *J. Mater. Civ. Eng.* **2013**, *25*, 781–787. [CrossRef]
27. Nath, P.; Sarker, P.K. Effect of GGBFS on Setting, Workability and Early Strength Properties of Fly Ash Geopolymer Concrete Cured in Ambient Condition. *Constr. Build. Mater.* **2014**, *66*, 163–171. [CrossRef]
28. Olivia, M. Durability Related Properties of Low Calcium Fly Ash Based Geopolymer Concrete. Ph.D. Thesis, Curtin University, Perth, Australia, 2011.
29. Carino, N.J. Nondestructive Techniques to Investigate Corrosion Status in Concrete Structures. *J. Perform. Constr. Facil.* **1999**, *13*, 96–106. [CrossRef]
30. Zaki, A.; Chai, H.K.; Aggelis, D.G.; Alver, N. Non-Destructive Evaluation for Corrosion Monitoring in Concrete: A Review and Capability of Acoustic Emission Technique. *Sensors* **2015**, *15*, 19069–19101. [CrossRef]
31. ASTM. C876-91(1999). *Standard Test Method for Half-Cell Potentials of Uncoated Reinforcing Steel in Concrete (Withdrawn 2008)*; ASTM International: West Conshohocken, PA, USA, 1999.
32. Gunasekara, C.; Law, D.; Bhuiyan, S.; Setunge, S.; Ward, L. Chloride Induced Corrosion in Different Fly Ash Based Geopolymer Concretes. *Constr. Build. Mater.* **2019**, *200*, 502–513. [CrossRef]
33. Miranda, J.M.; Fernández-Jiménez, A.; González, J.A.; Palomo, A. Corrosion Resistance in Activated Fly Ash Mortars. *Cem. Concr. Res.* **2005**, *35*, 1210–1217. [CrossRef]
34. Gupta, R.; Rathod, H.M. Current State of K-Based Geopolymer Cements Cured at Ambient Temperature. *Emerg. Mater. Res.* **2015**, *4*, 125–129. [CrossRef]
35. Belforti, F.; Azarsa, P.; Gupta, R.; Dave, U. Effect of Freeze-Thaw on K-Based Geopolymer Concrete (GPC) and Portland Cement Concrete (PCC). In Proceedings of the Technology Drivers: Engine for Growth: Proceedings of the 6th Nirma University International Conference on Engineering (NUiCONE 2017), Ahmedabad, India, 23–25 November 2017; CRC Press: Boca Raton, FL, USA, 2018; p. 65.

36. Yang, C. *Prediction of the Compressive Strength from Resonant Frequency for Low-Calcium Fly Ash-Based Geopolymer Concrete*; University of Victoria: Victoria, BC, Canada, 2017.
37. Gadve, S.; Mukherjee, A.; Malhotra, S.N. Corrosion of Steel Reinforcements Embedded in FRP Wrapped Concrete. *Constr. Build. Mater.* **2009**, *23*, 153–161. [CrossRef]
38. Pradhan, B.; Bhattacharjee, B. Half-Cell Potential as an Indicator of Chloride-Induced Rebar Corrosion Initiation in RC. *J. Mater. Civ. Eng.* **2009**, *21*, 543–552. [CrossRef]
39. Leelalerkiet, V.; Kyung, J.-W.; Ohtsu, M.; Yokota, M. Analysis of Half-Cell Potential Measurement for Corrosion of Reinforced Concrete. *Constr. Build. Mater.* **2004**, *18*, 155–162. [CrossRef]
40. Millard, S.G.; Gowers, K.R.; Gill, J.S. Reinforcement corrosion assessment using linear polarisation techniques. In *Evaluation and Rehabilitation of Concrete Structures and Innovations in Design*; Malhotra, V.M., Ed.; American Concrete Institute: Detroit, MI, USA, 1991; pp. 373–394.
41. Rodríguez, G.R.; Aperador, W. Remote Monitoring Technique for Evaluation of Corrosion on Reinforced Concrete Structures. *Non-Destr. Test.* **2016**. [CrossRef]
42. Olivia, M.; Nikraz, H. Properties of Fly Ash Geopolymer Concrete Designed by Taguchi Method. *Mater. Design. (1980–2015)* **2012**, *36*, 191–198. [CrossRef]
43. Kupwade-Patil, K.; Allouche, E.N. Examination of Chloride-Induced Corrosion in Reinforced Geopolymer Concretes. *J. Mater. Civ. Eng.* **2013**, *25*, 1465–1476. [CrossRef]
44. Andrade, C.; Alonso, C. Corrosion Rate Monitoring in the Laboratory and On-Site. *Constr. Build. Mater.* **1996**, *10*, 315–328. [CrossRef]
45. Shaikh, F.U. Effects of Alkali Solutions on Corrosion Durability of Geopolymer Concrete. *Adv. Concr. Constr.* **2014**, *2*, 109. [CrossRef]
46. ASTM. *C694-90a(2016), Standard Test Method for Weight Loss (Mass Loss) of Sheet Steel During Immersion in Sulfuric Acid Solution*; ASTM International: West Conshohocken, PA, USA, 2016.
47. Reddy, D.V.; Edouard, J.B.; Sobhan, K.; Tipnis, A. Experimental Evaluation of the Durability of Fly Ash-Based Geopolymer Concrete in the Marine Environment. In Proceedings of the 9th Latin American & Caribbean Conference, Medellin, Colombia, 3–5 August 2011; pp. 3–5.
48. ASTM. *C78/C78M-18, Standard Test Method for Flexural Strength of Concrete (Using Simple Beam with Third-Point Loading)*; ASTM International: West Conshohocken, PA, USA, 2018.
49. Al-Azzawi, M.; Yu, T.; Hadi, M.N.S. Factors Affecting the Bond Strength Between the Fly Ash-Based Geopolymer Concrete and Steel Reinforcement. *Structures* **2018**, *14*, 262–272. [CrossRef]
50. Austin, S.A.; Lyons, R.; Ing, M.J. Electrochemical Behavior of Steel-Reinforced Concrete During Accelerated Corrosion Testing. *CORROSION* **2004**, *60*, 203–212. [CrossRef]
51. Bertolini, L. Steel Corrosion and Service Life of Reinforced Concrete Structures. *Struct. Infrastruct. Eng.* **2008**, *4*, 123–137. [CrossRef]
52. Alanazi, H.; Yang, M.; Zhang, D.; Gao, Z. (Jerry) Early Strength and Durability of Metakaolin-Based Geopolymer Concrete. *Mag. Concr. Res.* **2016**, *69*, 46–54. [CrossRef]